Sensors and Materials, Vol. 33, No. 9 (2021) 3201–3212
MYU Tokyo

S & M 2681

Preparation of Oxidation-resistant Conductive Film Using Silver Nanowires and Reduced Graphene Oxide

Wei-Min Chiu,[1,2] Chane-Yuan Yang,[1*] Meng Ting Hsieh,[1] and Yu-Shu Chien[1]

[1]Chemical and Materials Engineering, National Chin-Yi University of Technology, Taiping District, Taichung 411030, Taiwan
[2]Graduate Institute of Precision Manufacturing, National Chin-Yi University of Technology, Taiping District, Taichung 411030, Taiwan

(Received June 9, 2021; accepted August 4, 2021)

Keywords: silver nanowires, reduced graphene oxide, AgNWs/RGO composite film, anti-oxidation

In this study, a highly stable and flexible silver nanowires (AgNWs)/reduced graphene oxide (RGO) composite transparent conductive film (TCF) was obtained by coating a solution of AgNWs and graphene oxide (GO) on polyethylene terephthalate (PET) with citrate reduction of GO. The AgNWs were synthesized by the microwave-heating polyol method, whereas GO was prepared by Hummer's method. The synthesis parameters of interest include microwave power and reaction time. The surface morphologies of the AgNWs and GO were investigated by scanning electron microscopy (SEM) and transmission electron microscopy (TEM), whereas the synthesized nanocomposite was characterized by X-ray diffractometry (XRD), Raman spectroscopy, and Fourier-transform infrared (FT-IR) spectroscopy. The experimental results showed that the suitable conditions of microwave heating for AgNW synthesis were 600 W and 40 min. The measurement of optoelectronic properties showed that the light transmittance of AgNWs was 80.13%, which is slightly higher than the requirement of TCFs of 80%. The sheet resistances of AgNWs without and with 3 wt.% RGO were 205.26 and 180.22 Ω/sq, respectively. Furthermore, the film stability was investigated in the ambient air, moist, and acetone environments. The increase in the AgNW sheet resistance after five weeks in the atmosphere was 123.2%, whereas with RGO protection, the increases in the sheet resistance were as low as 16.5, 27.3, and 48.1% in the ambient air, moist, and acetone environments, respectively. On the other hand, no significant variation of sheet resistance was detected even after the film was subjected to bend loading. It was thus shown that RGO can be used as a protective layer of AgNWs and that flexible AgNWs/RGO TCFs have the potential to be widely used in the optoelectronic industry.

1. Introduction

Recently, the rapid development of the electronics industry has triggered the extensive use of transparent conductive films (TCFs) in many domains, such as touch screens, panel displays, solar cells, and organic light-emitting diodes, owing to their excellent optical transparency and

*Corresponding author: e-mail: cyyang@ncut.edu.tw
https://doi.org/10.18494/SAM.2021.3437

ISSN 0914-4935

high conductivity.[1] The main material of TCFs is indium tin oxide (ITO), which has three major disadvantages: (1) the manufacturing process is complex and likely results in environmental pollution; (2) indium is a rare metal that is difficult to procure and relatively costly; and (3) ITO is a brittle material that is inapplicable to flexible TCFs. Therefore, much effort has been devoted to finding alternative materials to replace ITO for the more extensive use of TCFs in other electrical products. Owing to its aspect ratio,[2] excellent thermal and electrical conductivity, high light transmittance, and satisfactory flexibility,[3–5] silver nanowires (AgNWs) have been considered as a suitable candidate for transparent films. AgNWs have one-dimensional structures with a very high aspect ratio, a diameter of 10–200 nm, and a length of 5–100 μm. A wide range of AgNW applications includes smart sensors,[6–8] wearable sensors,[9,10] and soft e-skin.[11]

On the other hand, the metal meshes of AgNWs provide a conductive path for electrons through a continuous metal grid, and the light transmittance of a AgNWs film can be controlled by regulating the metal grid gap. The transmittance of AgNWs is normally higher than 80%, making them a potential replacement for expensive ITO for manufacturing flexible TCFs in the electronics industry.

However, the application of AgNWs as TCFs is also limited. The relatively high roughness of AgNW-based TCFs usually leads to the short circuit of devices. On the other hand, the conductivity of AgNW-based devices is normally affected by the resistance resulting from the large amount of contact between AgNWs. In addition, AgNWs, like other metals, are easily oxidized in ambient air, resulting in reduced TCF performance and the failure of devices.[12,13] Thus, the selection of protective materials for AgNWs[14,15] is an important topic.

Recently, graphene-based materials, such as graphene, graphene oxide (GO), and reduced graphene oxide (RGO), have attracted considerable attention as candidates for TCFs in view of their high electrical conductivity, high carrier mobility, and relatively high optical transmittance for visible light.[16,17] Graphene is a two-dimensional structure of carbon atoms arranged in a honeycomb with good characteristics, such as mechanical strength, thermal conductivity, electrical conductivity, and optical properties.[18] Graphene has been extensively used in touch screens,[19] conductive films,[20] chemical sensors, [21] solar cells,[22] and so forth. GO, containing only one or a few layers of carbon atoms such as graphene layers, is a new type of carbon material that possesses a high specific surface area and rich surface functional groups, as a result of which, its properties are different from those of graphene. There are three methods of preparing GO, namely, Brodie's method,[23] Staudenmaier's method,[24] and Hummer's method.[25] On the other hand, part of GO can be reduced to graphene-like sheets by removing the oxygen-containing groups that result in interlayer defects to obtain RGO. RGO has similar properties to graphene but includes oxygen-containing functional groups and structural defects.

Recently, it has been reported that GO[13,26,27] and RGO[28,29] can be used to protect AgNWs, not only by preventing the oxidation of AgNWs[30] and the failure caused by external forces, but also by reducing the roughness of the film surface to enhance the anti-oxidation and electrical conductivity of nano-Ag without affecting its transmittance.[29,31]

In this work, a highly stable and flexible AgNWs/RGO composite TCF was fabricated by coating a AgNWs/GO solution on polyethylene terephthalate (PET). AgNWs were synthesized

by the polyol method[5] with microwave heating, whereas GO was prepared by Hummer's method.[25] The AgNWs/GO mixture on the PET film was processed by citrate reduction[32] to obtain a AgNWs/RGO conductive composite film. The structure and photoelectrical properties of the as-prepared products were then characterized and measured. The remainder of this paper is organized as follows. Section 2 describes the experiment. In Sect. 3, the characterization and analysis of nanowires and composite films are presented, which is followed by the conclusion in Sect. 4.

2. Materials and Methods

2.1 Materials

The materials used in this study include silver nitrate ($AgNO_3$, 99.9%), ethylene glycol [EG, 99% $C_2H_4(OH)_2$], sodium chloride (99.5% NaCl), PVP (MW = 360000, 25%), graphite, sulfuric acid (98% H_2SO_4), and potassium permanganate (99% $KMnO_4$). All of the reagents were directly used without further purification.

2.2 Synthesis of AgNWs

The synthesis process started from the dissolution of $AgNO_3$ and NaCl in EG, then the solution was heated by microwaves at 160 °C for 3 min to form the crystal seeds. Thereafter, the solutions of $AgNO_3$ and PVP in EG were added to the silver crystal seed solution. The mixture was heated again by microwaves at 160 °C. The solution was then cooled to room temperature and washed with pure EG. Finally, the precipitate of AgNWs was obtained by repeated centrifugation.

2.3 Preparation of GO

In this work, GO was prepared by Hummer's method,[25] in which graphite was first dissolved in H_2SO_4, then mixed with slowly added $KMNO_4$ solution. The mixture was stirred in an ice bath for 5 days. After that, 5% H_2SO_4 solution was added and the mixture was stirred for 2 h, followed by mixing with 30% aqueous H_2O_2 solution. Excess metal ions in the solution were removed by washing several times with aqueous H_2SO_4 solution and then with DI water to ensure neutrality. Thereafter, the precipitate of GO was obtained by freeze drying.

2.4 Preparation of composite film

The performance of materials or devices composed of RGO is determined by the reduction processes of GO.[33] To prepare the AgNWs/RGO composite in a film shape, the AgNW solution obtained previously was mixed with a GO solution and oscillated by an ultrasonic oscillator for 30 min to disperse the suspension. Thereafter, the solution was coated on a PET substrate to form a composite film, which was then placed in a circulation oven and reduced in sodium

citrate ($Na_3C_6H_5O_7$)[32] vapor at 90 °C for 10 h to produce the AgNWs/RGO film. The AgNW, the GO, and the composite AgNWs/RGO conductive films were then characterized and measured.

3. Results and Discussion

3.1 Characterization of AgNWs

In this study, microwave heating was used to synthesize AgNWs, and the effect of the microwave power[34,35] and heating time[34] on their growth was investigated. Yi *et al.*[34] employed microwave radiation and chemical modification (NaBr) in the polyol method, in which different microwave powers resulted in different temperatures and reaction rates, and accordingly nano-Ag products with different structures, including irregular, linear, and particular products.[34] In what follows, the analysis of AgNWs synthesized under various conditions is presented.

3.1.1 Scanning electron microscopy (SEM)

The effect of the microwave power on the growth of the nanowires was investigated via three microwave powers (400, 600, and 800 W) applied for 20 min. The morphology of AgNWs was observed by field emission SEM (FE-SEM) (JSM-6360, JEOL) with a 10–15 kV voltage. Figures 1(a)–1(c) show SEM images of AgNWs synthesized with microwave powers of 400, 600, and 800 W, respectively. As shown in Fig. 1(a), the structures of the nanowires synthesized at 400 W were mainly granular and linear, indicating that the nanowires were not effectively synthesized owing to the low reaction rate. Figure 1(b) shows that the structure of the AgNWs synthesized at 600 W was mainly linear. The average length was about 20 μm and the diameter was about 100 nm. Figure 1(c) shows the product of AgNWs synthesized at 800 W, demonstrating that the AgNWs wires did not grow longer at such a high power. This is due to the overheating caused by the excessively high reaction rate; the local structure of the AgNWs was therefore damaged after the complete growth, leading to rod-shaped and granular products. The results indicated that the most suitable microwave power for the formation of linear AgNWs was 600 W in this work.

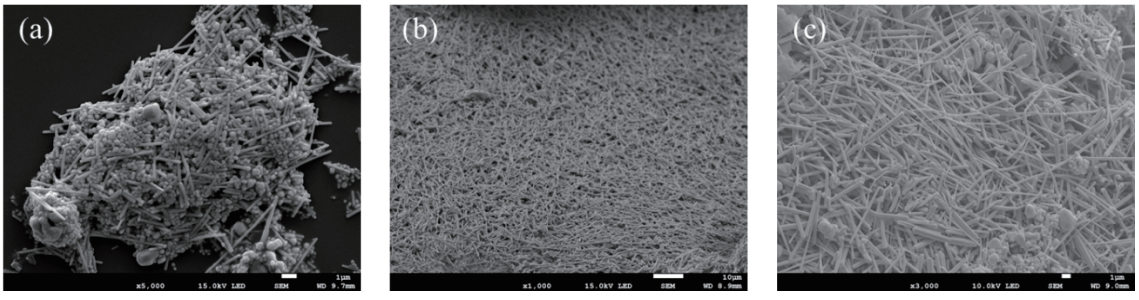

Fig. 1. SEM images of the AgNWs grown at microwave powers of (a) 400, (b) 600, and (c) 800 W for 20 min.

Next, AgNWs were synthesized at a microwave power of 600 W for 10, 20, 40, and 60 min to investigate the effect of the heating time on the AgNW crystallization. Figure 2(a) shows the product heated for 10 min. It can be seen that most nanowires were granular and rod-like due to the insufficient heating time and, accordingly, the uncompleted reaction. From Fig. 2(b), it was found that most of the products formed with 20 min of heating were wires of 10 μm average length. Figure 2(c) shows that 40 min of heating results in the growth of linear nanowires with an average length of 20 μm. Finally, in the case of heating for 60 min [Fig. 2(d)], it was found that the AgNWs were broken, reducing their length. This can be explained by considering that the conductive electrons were polarized by the oscillating microwave field. If the reaction time is too long or the reaction is too fast, the induced electron polarization and charge localization may lead to overheating,[33] resulting in a damaged product with shorter rods or granular particles. To summarize, the best conditions of microwave heating for the growth of AgNWs were 600 W power and 40 min of heating, which were next employed to prepare composite conductive films.

3.1.2 X-ray diffractometry (XRD)

The crystalline phase of the AgNWs was observed by XRD (X'Pert^3 Powder). As shown in Fig. 3, four characteristic peaks were found at 38.2, 44.5, 64.6, and 77.5°, corresponding to the diffraction of the (111), (200), (220), and (311) crystal faces of the AgNWs, respectively. The XRD pattern indicates that the AgNWs had a face-centered cubic (fcc) structure. Furthermore, the ratio of the two peaks (111) and (200) verified the excellent aspect ratio of the AgNWs.

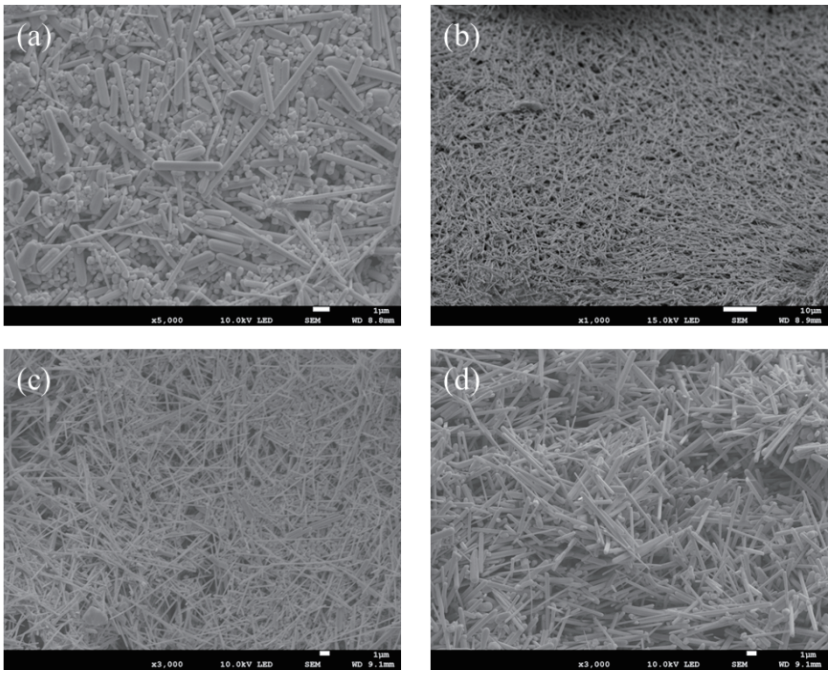

Fig. 2. SEM images of the AgNWs grown at 600 W for (a) 10, (b) 20, (c) 40, and (d) 60 min.

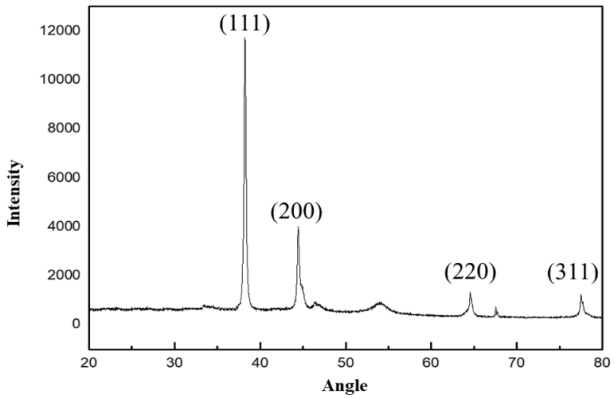

Fig. 3. XRD pattern of the AgNWs. Characteristic peaks were found at 38.2, 44.5, 64.6, and 77.5°, corresponding to the (111), (200), (220), and (311) crystal faces, respectively.

3.1.3 Sheet resistance and transmittance

The sheet resistance of AgNWs was measured by a four-point probe (5601Y) to investigate the electrical conductivity. On the other hand, the transmittance of AgNWs was measured using a haze meter (NDH2000). Figure 4 shows the effect of the AgNW concentration on both the sheet resistance and transmittance. At high concentrations such as 8 and 10 wt.%, the AgNWs were tightly packed, resulting in high electrical conductivity and excellent ability to transfer electronic information. However, the tightly packed AgNWs had few gaps and consequently low transmittance. At the concentration of 6 wt.%, the transmittance remained higher than 80%, meeting the requirement of the relatively low sheet resistance for TCFs. Therefore, in the subsequent experiments, 6 wt.% AgNWs were used with GO to fabricate the composite conductive films.

On the other hand, silver is easily oxidized when exposed to the atmosphere, resulting in the deterioration of conductivity. In this study, the composite films were exposed to ambient air for up to five weeks, during which their sheet resistance was measured once a week. The results in Fig. 5 show that the sheet resistance increased with the time of exposure to air, confirming that the AgNW films with different Ag contents were oxidized in the atmosphere. To prevent the oxidation of AgNWs, RGO was used as the protective layer of the AgNWs used to fabricate the composite conductive film.

3.2 Properties of GO

3.2.1 Transmission electron microscopy (TEM)

The morphology of GO was observed by TEM (H-7500, HITACHI) with an 80 kV working voltage. The structure of GO was characterized by the color in the TEM image as shown in Fig. 6. It can be seen that there were about four layers in the lamellar structure of GO, identifying it as few-layer GO.

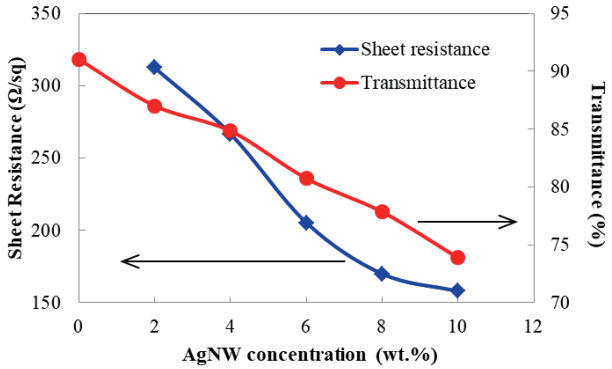

Fig. 4. (Color online) Effect of AgNW content on the sheet resistance and transmittance of TCFs.

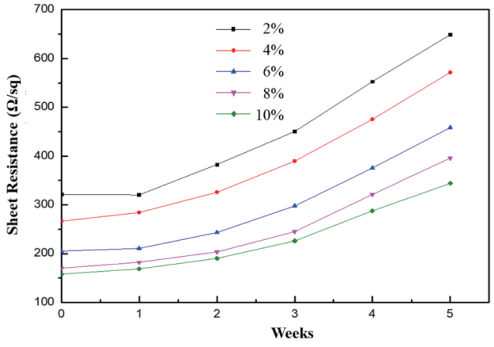

Fig. 5. (Color online) Effect of AgNW concentration on the sheet resistance of TCFs over five weeks.

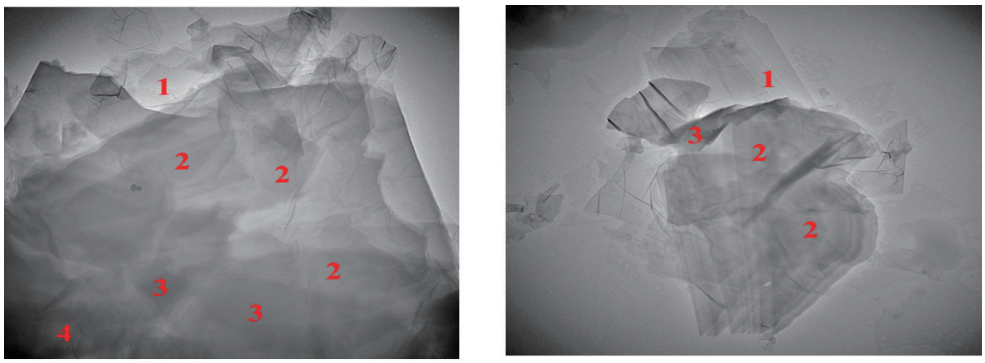

Fig. 6. (Color online) TEM image of GO, showing the existence of approximately four layers.

3.2.2 Raman spectrometer

A Raman spectrometer (JOBIN-YVON T64000), which is widely used in the characterization of carbon-based materials,[36] is an ideal instrument for analyzing the defects of GO.[37] As shown in Fig. 7, two peaks, representing graphite and GO, were found in the Raman spectra. The *D* peaks, representing the defect band, were found at 1334.88 and 1577.52 cm^{-1} for graphite and GO, whereas the *G* peaks, i.e., the optical phonons of carbon atoms moving in the opposite phase, were found at 1336.70 and 1593.26 cm^{-1} for graphite and GO, respectively. The right shift of the *G* band of GO indicates a GO structure of less than 10 layers.[38] Moreover, the defect density of GO can be investigated via the ratio of the Raman peak heights I_D/I_G based on the Tuinstra–Koenig law, which relates the crystallite size to the ratio of Raman peak heights.[39] In this study, the *D* and *G* peak heights were 147.04 and 477.86 for and 1200.59 and 983.79 for GO, resulting in I_D/I_G values of 0.31 and 1.22 for the original graphite and GO, respectively. It was verified that the structure of the graphite surface was destroyed by the mixed acid and strong oxidizing agent, which produced oxygen-containing functional groups and defects on the graphite surface during the chemical intercalation process.

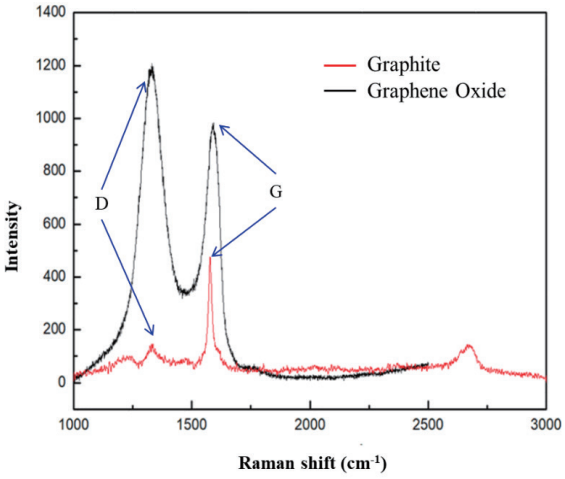

Fig. 7. (Color online) Raman spectra of graphite and GO.

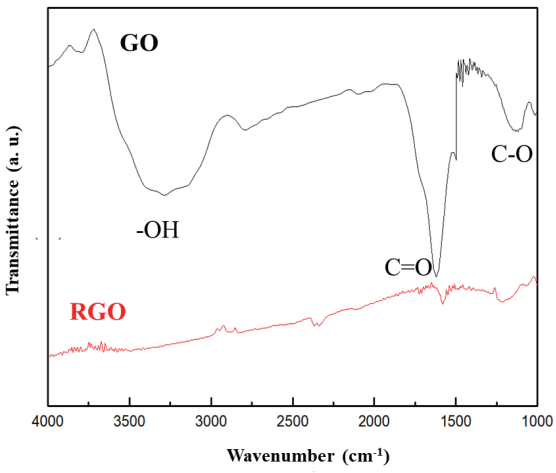

Fig. 8. FTIR spectra of GO and RGO.

3.2.3 Fourier-transform infrared (FT-IR)

FTIR (IRAffinity-1, Shimadzu) was used to analyze oxygen-containing functional groups on GO. Figure 8 shows the FTIR spectrum of GO, in which the absorption peaks found at 3435 and 1718 cm^{-1} represent the hydrogen bond generated between the GO layers and the stretching vibration of C=O, respectively. The peak found at 1153 cm^{-1} represents the bending vibration of C–O in the C–OH functional group and the C–O stretching vibration of the epoxide group. It was therefore verified that the GO prepared in this study included the oxygen-containing functional groups such as hydroxyl, carbonyl, and epoxide groups.

Meanwhile, the RGO was also identified by FTIR via the analysis of the functional groups as shown in Fig. 8. The CO characteristic peaks were clearly weakened and the –OH characteristic peak was found to vanish due to the reduction of GO, indicating the effect of sodium citrate on the reduction of GO.

3.3 Properties of composite film

In this study, RGO of different concentrations was used as a protective agent to prevent the oxidation of AgNWs. Moreover, since the conductivity of graphene is inherently excellent, the conduction of AgNWs can also be improved. As shown in Fig. 9, the greater the RGO concentration in the composite, the lower the sheet resistance. The sheet resistance of the original AgNWs was 205.26 Ω/sq, which decreased to 180.22 with 3 wt.% RGO. On the other hand, the electrical resistance decreased significantly above an RGO concentration of 1 wt.%, and the light transmittance was also deteriorated by RGO. When the RGO content was 1 wt.%, the transmittance was still higher than 80%, but it decreased from 80.13% with 1 wt.% RGO to 65.88% with 3 wt.% RGO.

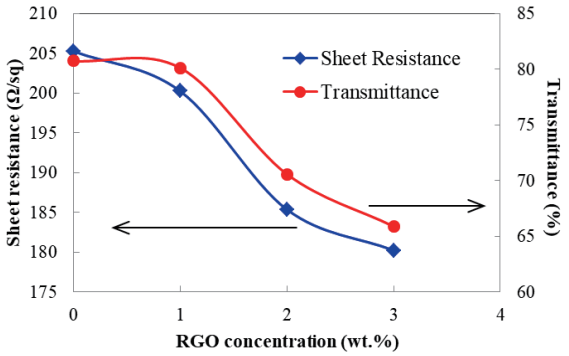

Fig. 9. (Color online) Effect of RGO concentration on the sheet resistance and transmittance of AgNWs/RGO composite film.

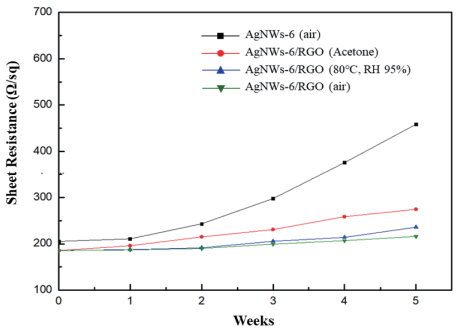

Fig. 10. (Color online) Variation of sheet resistance of AgNWs/RGO films in different environments.

Note that Naito *et al.*[40] applied the diluted suspension of the GO twice to prepare the TCFs of AgNW sandwiched by GO. The sheet resistance of the composite film was improved to 10.4 Ω/sq. Kumar *et al.*[41] proposed to apply sequentially three post-processing methods: thermal embossing, photonic sintering, and N_2 plasma treatment of AgNW TCFs, leading to a sheet resistance of 2.5 Ω/sq. These sheet resistances were much lower than those of AgNW TCFs synthesized by the polyol method in the present work. However, in view of simplicity, control, yield, and cost, the polyol method is considered as the most promising for AgNWs synthesis.

On the other hand, to investigate the protective ability of RGO in the application environments, we monitored the sheet resistance of AgNWs/RGO composite films in various environments for up to five weeks as shown in Fig. 10. When the original AgNW film was placed in ambient air for five weeks, the increase in the sheet resistance was 123.2%. With the addition of RGO, the increase in the sheet resistance dropped to 16.5%, indicating the capability of RGO in preventing the oxidation of nanowires. Furthermore, the chemical resistance of the composite film was tested by placing it in an acetone environment, which resulted in a 48.1% increase in the sheet resistance. In addition, the conductive composite film was tested in an environment of 80 °C and RH 95% to evaluate its weather resistance. The increase in the sheet resistance was 27.3%.

The experimental results verified the protective effect of RGO on the oxidation of AgNWs. Moreover, the conductive AgNWs/RGO composite films remained stable in the test environments, showing their suitability for use as composite conductive films.

3.3.1 TEM

From the analysis of AgNWs/RGO film transmittance, it was found that the light transmittance decreased upon the addition of excess RGO. The stacking of graphene with different concentrations can be seen in TEM images in Fig. 11. The silver content was 6 wt.%

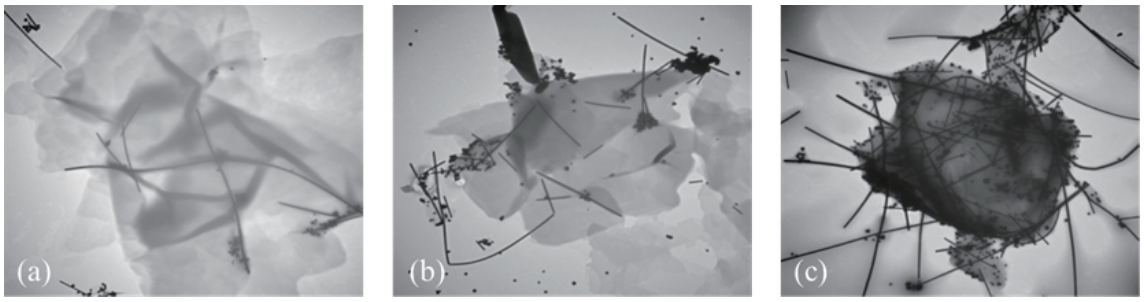

Fig. 11. TEM images of the structure of AgNWs/RGO composite film with RGO content: (a) 1, (b) 2, and (c) 3 wt.%.

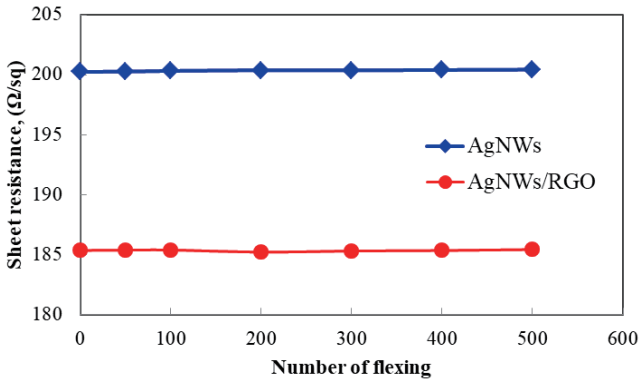

Fig. 12. (Color online) Results of flexural test of AgNWs and AgNWs/RGO composite films.

and RGO concentrations were 1, 2, and 3 wt.%. Clearly, the greater the RGO content, the lower the light transmittance of the composite film. This indicated that the transmittance was deteriorated by the addition of RGO.

3.3.2 Flexure test

In addition to preparing a composite conductive film with oxidation resistance, an aim of the present work was to develop a flexible conductive film. It was found that RGO not only prevents the oxidation of AgNWs but also improves the adhesion of AgNWs on the substrate by tightly covering the AgNWs on the substrate.[26] In this work, flexural tests were conducted to investigate the flexibility of AgNWs/RGO TCFs. As shown in Fig. 12, after flexing the films 500 times, the composite sheet resistance remained stable, indicating that the as-prepared AgNWs/RGO composite can indeed be used to prepare flexible conductive films.

4. Conclusions

In this work, conductive AgNWs/RGO composite films were prepared in three steps: (1) synthesis of AgNWs by the microwave-heating polyol method, (2) synthesis of GO by Hummer's

method, and (3) preparation of a transparent conductive composite film of nanowires and reduced GO on PET. The AgNWs, GO, and AgNWs/RGO films were characterized to investigate their performance. The results showed that the most suitable conditions for AgNW synthesis were a microwave power of 600 W with heating for 40 min, for which the product mostly had a linear structure with a length of about 20 μm and a diameter of about 100 nm. On the other hand, it was found that the higher the concentration of AgNWs, the higher the conductivity but the lower the light transmittance. In the case of 6 wt.% AgNW, the light transmittance remained higher than 80%, meeting the requirement of TCFs, with relatively good conductivity observed at this and other concentrations.

TEM images of GO show that the number of layers of the prepared GO was about four FTIR analysis revealed obvious absorption peaks of GO at 3435, 1718, and 1153 cm^{-1}, indicating that oxygen-containing groups were indeed connected between the graphite layers. It was also found that the synthesized product was a few layers of GO. The conductivity of the AgNWs/RGO composite conductive film was higher than that of the original AgNW wire film. After five weeks of oxidation under suitable conditions to evaluate the solvent resistance and weather resistance of the AgNWs/RGO films, it was found that RGO played an important role as an effective protective layer for AgNWs. Furthermore, a flexure test showed no significant variation in the electric resistance even when the film was subjected to bend loading, verifying that AgNWs/RGO composite films can be used as flexible conductive films to replace ITO films in the optoelectronic industry.

References

1 Y. S. Yun, D. H. Kim, B. Kim, H. H. Park, and H.-J. Jin: Synth. Met. **162** (2012) 1364. https://doi.org/10.1016/j.synthmet.2012.05.026
2 Y. Zhang, J. Wang, and P. Yang: Mater. Res. Bull. **48** (2013) 461. https://doi.org/10.1016/j.materresbull.2012.11.011
3 C.-H. Chung, T.-B. Song, B. Bob, R. Zhu, and Y. Yang: Nano Res. **5** (2012) 805. https://doi.org/10.1007/s12274-012-0264-8
4 S. J. Henley, M. Cann, I. Jurewicz, A. Daltonc, and D. Milne: Nanoscale **6** (2013) 946. https://doi.org/10.1039/c3nr05504c
5 P. Zhang, I. Wyman, J. Hua, S. Lin, Z. Zhong, Y. Tu, Z. Huang, and Y. Wei: Mater. Sci. Eng., B **223** (2017) 1. https://doi.org/10.1016/j.mseb.2017.05.002
6 L. Wang, X. Gao, L. Jin, Q. Wu, Z. Chen, and X. Lin: Sens. Actuators, B **176** (2013) 9. https://doi.org/10.1016/j.snb.2012.08.077
7 R. S. Jones, R. R. Draheim, and M. Roldo: Appl. Sci. **8** (2018) 673. https://doi.org/10.1002/adma.201505559
8 P. S. Karthik and S. P. Singh: RSC Adv. **5** (2015) 77760. https://doi.org/10.1039/C5RA12013F
9 J. Kim and W. S. Kim: Sens. Actuators, A **238** (2016) 329. https://doi.org/10.1016/j.sna.2015.12.030
10 A. C. Myers, H. Huang, and Y. Zhu: RSC Adv. **5** (2015) 11627. https://doi.org/10.1039/C4RA15101A
11 R. Dahiya, N. Yogeswaran, F. Liu, L. Manjakkal, E. Burdet, V. Hayward, and H. Jörntell: Proc. IEEE **107** (2019) 2016. https://doi.org/10.1109/JPROC.2019.2941366
12 S.-B. Yang, H. K. Choi, D. S. Lee, C.-G. Choi, S.-Y. Choi, and I.-D. Kim: Small **11** (2015) 1293. https://doi.org/10.1002/smll.201402474
13 C. Wu, J. Jiu, T. Araki, H. Koga, T. Sekitani, H. Wang, and K. Suganuma: RSC Adv. **6** (2016) 15838. https://doi.org/10.1039/C5RA24896E
14 B. Zhang, D. Liu, Y. Liang, D. Zhang, H. Yan, and Y. Zhang: Mater. Lett. **201** (2017) 50. https://doi.org/10.1016/j.matlet.2017.04.137
15 P. Meenakshi, R. Karthick, M. Selvaraj, and S. Ramu: Sol. Energy Mater. Sol. Cells **128** (2014) 264. https://doi.org/10.1016/j.solmat.2014.05.013
16 W. Xiong, H. Liu, Y. Chen, M. Zheng, Y. Zhao, X. Kong, Y. Wang, X. Zhang, X. Kong, P. Wang, and L. Jiang: Adv. Mater. **28** (2016) 7167. https://doi.org/10.1002/adma.201600358

17 L. Cai, S. Zhang, Y. Zhang, J. Li, J. Miao, Q. Wang, Z. Yu, and C. Wang: Adv. Mater. Technol. **3** (2018) 1700232. https://doi.org/10.1002/admt.201700232
18 S. Korkmaz and A. Kariper: J. Energy Storage **27** (2020) 101038. https://doi.org/10.1016/j.est.2019.101038
19 Z. Chen, Y. Liu, W. Zhang, X. Guo, L. Yin, Y. Wang, L. Li, Y. Zhang, Z. Wang, and T. Zhang: Mater. Chem. Phys. **221** (2019) 78. https://doi.org/10.1016/j.matchemphys.2018.09.039
20 Q. Zheng, Z. Li, J. Yang, and J. K. Kim: Prog. Mater. Sci. **64** (2014) 200. https://doi.org/10.1016/j.pmatsci.2014.03.004
21 S. Aslam, T. H. Bokhari, T. Anwar, U. Khan, A. Nairan, and K. Khan: Mater. Lett. **235** (2019) 66. https://doi.org/10.1016/j.matlet.2018.09.164
22 M. Sreejesh, N. M. Huang and H. S. Nagaraja: Electrochim. Acta **160** (2015) 94. https://doi.org/10.1016/j.electacta.2015.02.005
23 B. C. Brodie: Philos. Trans. R. Soc. **149** (2009) 249. https://doi.org/10.1098/rstl.1859.0013
24 L. Staudenmaier: Eur. J. Inorg. Chem. **32** (2010) 1394. https://doi.org/10.1002/cber.18980310237
25 W. S. Hummers Jr. and R. E. Offeman: J. Am. Chem. Soc. **80** (1958) 1339. https://doi.org/10.1021/ja01539a017
26 G. Eda and M. Chhowalla: Adv. Mater. **22** (2010) 2392. https://doi.org/10.1002/adma.200903689
27 J. Liang, L. Li, K. Tong, Z. Ren, W. Hu, X. Niu, Y. Chen, and Q. Pei: ACS Nano **8** (2014) 1590. https://doi.org/10.1021/nn405887k
28 Y. Ahn, Y. Jeong, and Y. Lee: ACS Appl. Mater. Interfaces **4** (2012) 6410. https://doi.org/10.1021/am301913w
29 P. Meenakshi, R. Karthick, M. Selvaraj, and S. Ramu: Sol. Energy Mater. Sol. Cells **128** (2014) 264. https://doi.org/10.1016/j.solmat.2014.05.013
30 J. Kim, L. J. Cote, F. Kim, W. Yuan, K. R. Shull, and J. Huang: J. Am. Chem. Soc. **132** (2010) 8180. https://doi.org/10.1021/ja102777p
31 D. Lee, H. Lee, Y. Ahn, Y. Jeong, D.-Y. Lee, and Y. Lee: Nanoscale **5** (2013) 7750. https://doi.org/10.1039/c3nr02320f
32 C. Shen and S. Olutunde Oyadiji: Mater. Today Phys. **15** (2020) 100257. https://doi.org/10.1016/j.mtphys.2020.100257
33 S. Pei and H.-M. Cheng: Carbon **50** (2012) 3210. https://doi.org/10.1016/j.carbon.2011.11.010
34 Z. Yi, X. Xu, X. Tan, L. Liu, W. Zhang, Y. Yi, J. Luo, W. Yao, Y. Yi, T. Duan, and Y. Tang: Surf. Coat. Tech. **327** (2017) 118. https://doi.org/10.1016/j.surfcoat.2017.08.024
35 Y. Yang, Y. Hu, X. Xiong, and Y. Qin: RSC Adv. **3** (2013) 8431. https://doi.org/10.1039/C3RA00117B
36 T. Jawhari, A. Roid, and J. Casado: Carbon **33** (1995) 1561. https://doi.org/10.1016/0008-6223(95)00117-V
37 A. C. Ferrari, J. C. Meyer, V. Scardaci, C. Casiraghi, M. Lazzeri, F. Mauri, S. Piscanec, D. Jiang, K. S. Novoselov, S. Roth, and K. Geim: Phys. Rev. Lett. **97** (2006) 187401. https://doi.org/10.1103/PhysRevLett.97.187401
38 A. Gupta, G. Chen, P. Joshi, S. Tadigadapa, and P. C. Eklund: Nano Lett. **6** (2006) 2667. https://doi.org/10.1021/nl061420a
39 F. Tuinstra and J. L. Koenig: J. Chem. Phys. **53** (1970) 1126. https://doi.org/10.1063/1.1674108
40 K. Naito, R. Inuzuka1, N. Yoshinaga, and W. Mei: Synthetic Metals **237** (2018) 50. https://doi.org/10.1016/j.synthmet.2018.02.004
41 D. Kumar, V. Stoichkov, E. Brousseau, G. C. Smith, and J. Kettle: Nanoscale **11** (2019) 5760. https://doi.org/10.1039/c8nr07974a